Energy Maximization Absorption of Wave Energy Converter Based on Fourier Pseudo-Spectral Method and Adaptive Dynamic Programming

Xinyu Bao, Zhen Chen, and Ming Li

***Abstract*—In this paper, we propose a novel noncausal control framework to address the energy maximization problem of wave energy converters (WECs) subject to constraints. The energy maximization problem of WECs is a constrained optimal control problem. The proposed control framework converts this problem into a reference trajectory tracking problem through the Fourier pseudo-spectral method (FPSM) and utilizes the online tracking adaptive dynamic programming (OTADP) algorithm to realize real-time trajectory tracking for practical use in the ocean environment. Using the wave prediction technique, the optimal trajectory is generated online through a receding horizon (RH) implementation. A critic neural network (NN) is applied to approximate the optimal cost value function and calculate the error-tracking control by solving the associated Hamilton-Jacobi-Bellman (HJB) equation. The proposed WEC control framework improves computational efficiency and makes the online control feasible in practice. Simulation results show the effects of the receding horizon implementation of FPSM with different window lengths and window functions, while verifying the performances of tracking control and energy absorption of WECs in two different sea conditions.**

***Index Terms*—Wave energy converter, Fourier pseudo-spectral control, adaptive dynamic programming, energy maximization, optimal trajectory tracking control**

I. INTRODUCTION

Renewable energy can fill the gap between energy consumption and carbon reduction to achieve carbon neutrality [1]. Compared with other types of renewable energy such as solar and wind energy, wave energy can potentially provide about 32,000 TWh/year [2]. To harness wave energy, different types of wave energy converters (WECs) have been developed over the past decades [3]. However, due to the high levelized cost of energy (LCoE), the WEC technologies remain immature for commercial use [1].

Reducing the LCoE of WECs depends on both a well-designed device and a reliable control approach. It is acknowledged that the development of control strategies is crucial in increasing the energy conversion efficiency and ensuring the security of WECs. The classical control methods such as latching control [4] and declutching control [5], based on the complex-conjugate impedance matching principle, are applied to make WEC resonate with the dominant frequency of incoming ocean waves. Since these approaches address a single frequency, they are not feasible for realistic irregular ocean waves with multiple frequencies [6].

The maximum energy absorption problem of WECs is essentially an optimal control problem with physical constraints [7]. With the ability to incorporate constraints into the optimal control problem, model predictive control (MPC) can be employed to maximize the energy absorption of WEC. However, this becomes numerically intractable because it involves solving a non-convex optimization problem. To address this issue, additional terms are added to the objective function to ensure the convex property [8–10]. At the cost of handling the constraint implicitly, dynamic programming (DP) is utilized to control the WEC systems [11–13]. DP is integrated into the economic MPC framework in Ref. [14] to stabilize WEC and to draw the maximum energy from it. However, both online implementation of MPC and DP-based nonlinear optimal control spawn large computational complexity, especially when the dynamics of WECs are described by a high-order model to maintain the modeling fidelity.

To tackle the issue of dimensionality of DP, adaptive dynamic programming (ADP) that combines the function approximator and reinforcement learning (RL) has been studied for decades [15–17]. Recently, the ADP approach has been utilized to address the problem of WEC energy maximization control. One of the earliest works presents an online ADP algorithm to ensure robustness against various forms of model uncertainty and constraints in a WEC system [18]. To address the nonlinearity of WECs, the causal and noncausal ADP algorithms are proposed respectively in Refs. [19, 20]. Nevertheless, the constraints are treated as the extra terms of cost function in these ADP algorithms that affect the real optimal extracted energy. In Refs. [21–23], some frequency-based methods such as pseudo-spectral and moment approaches are utilized to transform the original optimal problem into a convex form, so that the optimal

Manuscript received: 5 July 2024; revised: 3 August 2024; accepted: 23 August 2024. *(Corresponding author: Ming Li.)*

Citation: X. Bao, Z. Chen, and M. Li, Energy maximization absorption of wave energy converter based on Fourier pseudo-spectral method and adaptive dynamic programming, *IJICS*, 2024, 29(3), 108–118.

Xinyu Bao is with Department of Railway, Hohhot Vocational College, Hohhot 010000, China (e-mail: bxy_baoxinyu_0111@163.com).

Zhen Chen and Ming Li are with Automation and Measurement Department, Ocean University of China, Qingdao 266100, China (e-mail: oucchenzhen@ouc.edu.cn; limingneu@ouc.edu.cn).

Digital Object Identifier 10.62678/IJICS202409.10126

solution can be easily calculated. However, these works focus on optimal steady-state control and fail to consider the transient performance of WECs.

To improve the energy conversion efficiency of WECs and the computational speed, this paper proposes a novel two-level control framework that combines the Fourier pseudo-spectral method (FPSM) and online tracking ADP (OTADP) algorithm. By solving the energy maximization problem, the first-level accomplishes the real-time optimal reference trajectory generation through FPSM. Inspired by Ref. [24], the reference trajectory is generated in a receding horizon (RH) manner when considering the displacement constraints in every optimization. The second-level OTADP consists of a single critic neural network (NN) whose weights are tuned online, an ADP controller, and a steady-state controller to make WEC track the desired trajectory to absorb the maximum energy from ocean waves. The main contributions of this paper are as follows:

(1) In contrast to previous ADP algorithms that are applied to facilitate computation, the ADP controller in this paper is tailor-made to yield energy maximization of WEC device with guaranteed convergence of the algorithm and stability of the closed-loop control.

(2) Unlike the existing DP-based approach in WEC control systems, the proposed FPSM-OTADP handles the displacement constraints explicitly without the need of modifying the objective function. Further, the online reference trajectory generation is realized through an RH implementation.

The remainder of this paper is organized as follows. In Section II, we model the point absorber (PA) type of WEC used and provide equations of the energy maximization optimal problem for WECs. In Section III, the RH implementation of FPSM and the OTADP algorithm are described and the proof of stability of tracking-error system and convergence of critic NN weights is given using the Lyapunov function. Section IV shows the simulation results of the proposed method. Finally, Section V presents conclusions.

II. WEC Modeling and Problem Description

In this paper, the heaving point absorber, as shown in Fig. 1, serves as a benchmark device of WEC. As the controller of WEC, the power take-off (PTO) system converts the kinetic energy from the incident ocean waves to electric energy. We assume that the power conversion efficiency is 100%.

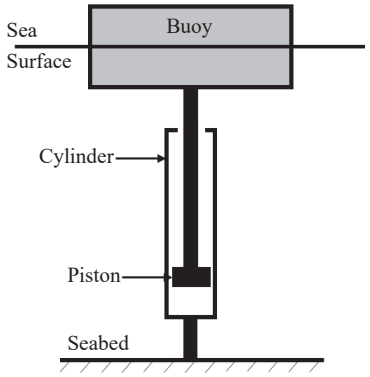

Figure 1 Heaving point absorber structure diagram.

When the heaving buoy is excited by incident waves, based on Newton's second law, the motion can be formulated as follows

$$m\ddot{z} = f_{\mathrm{s}} + f_{\mathrm{r}} + f_{\mathrm{e}} + f_{\mathrm{pto}} \tag{1}$$

where m is the buoy mass, z is the heaving displacement of the buoy, f_{s}, f_{r}, and f_{e} are the hydrostatic force, radiation force, and excitation force, and f_{pto} is the PTO force, respectively. Upward heaving motion is defined as the positive direction. The hydrostatic force f_{s} is calculated by

$$f_{\mathrm{s}} = -\rho g S z = -k_{\mathrm{hs}} z \tag{2}$$

where ρ is the density of water, g is the gravitational acceleration, S is the water plane area of the heaving buoy, and k_{hs} is the coefficient of the hydrostatic force, respectively. According to the Cummings equation [25], the radiation force f_{r} is determined as follows

$$f_{\mathrm{r}} = -m_{\infty}\ddot{z} - \int_{-\infty}^{t} k_{\mathrm{r}}(\tau - t)\dot{z}(\tau)\mathrm{d}\tau \tag{3}$$

where m_{∞} is the added mass at infinity frequency, τ is a variable in the integral formula, t means the time variable, and $k_{\mathrm{r}}(t)$ is the radiation impulse response function (IRF), which can be obtained with boundary element analysis software like NEMOH [26]. The convolutional term in Eq. (3), noted as f_{r1}, can be approximated by the finite-dimensional state-space model

$$\begin{aligned} \dot{x}_{\mathrm{r}} &= A_{\mathrm{r}} x_{\mathrm{r}} + B_{\mathrm{r}}\dot{z}, \\ f_{\mathrm{r1}} &= \int_{-\infty}^{t} k_{\mathrm{r}}(\tau - t)\dot{z}(\tau)\mathrm{d}\tau \approx C_{\mathrm{r}} x_{\mathrm{r}} \end{aligned} \tag{4}$$

where $x_{\mathrm{r}} \in \mathbb{R}^{n_{\mathrm{r}}\times 1}$ is an n_{r}-dimensional state vector, and $A_{\mathrm{r}} \in \mathbb{R}^{n_{\mathrm{r}}\times n_{\mathrm{r}}}$, $B_{\mathrm{r}} \in \mathbb{R}^{n_{\mathrm{r}}\times 1}$, and $C_{\mathrm{r}} \in \mathbb{R}^{1\times n_{\mathrm{r}}}$ are the state-space equation matrices. Substituting Eqs. (2) and (3) into Eq. (1), the dynamic equation of buoy of WEC is written as

$$m_{\mathrm{t}}\ddot{z} = -k_{\mathrm{hs}} z - f_{\mathrm{r1}} + f_{\mathrm{e}} + f_{\mathrm{pto}} \tag{5}$$

where $m_{\mathrm{t}} = m + m_{\infty}$ is the total mass. It should be noted that when the controlled WEC resonates with ocean waves, a small variation of control will induce a large motion. Therefore, to avoid allowing the buoy to fully submerge into water or jump out of the water, where a damage can be caused, the limitation of displacement z is necessary in designing controller.

The instant extracted power is computed as $P = -f_{\mathrm{pto}}\dot{z}$. To find the maximum average power, the control problem of WEC can be formulated as follows

$$\begin{aligned} &\max_{f_{\mathrm{pto}}} \frac{1}{T}\int_0^T -f_{\mathrm{pto}}\dot{z}\mathrm{d}t, \\ &\text{s.t.,}\quad \text{Eq. (5)}, \\ &z_{\min} \leqslant z \leqslant z_{\max} \end{aligned} \tag{6}$$

where T is the overall control horizon, and $z_{\max}$ and $z_{\min}$ are the upper bound and lower bound of z, respectively.

Based on Eq. (6), the control problems of WEC are summarized as follows:

(1) The constrained optimal control problem of WEC is solved without adding additional terms in the objective function.

(2) The real-time control for practical use is maintained under the persistent excitation (PE) of an ocean wave.

(3) When WEC resonates with a wave, the stability of the WEC system should be maintained.

III. FPSM-OTADP Framework

To complete the tasks proposed in Section II, a robust, self-learning control strategy FPSM-OTADP is designed in this section. The framework is shown in Fig. 2. First, we present the FPSM applied in WECs and the RH implementation of real-time trajectory generation (RTTG). Then, the OTADP algorithm is presented in detail. Finally, the proof of stability of the control system and the convergence of the critic NN weights is provided.

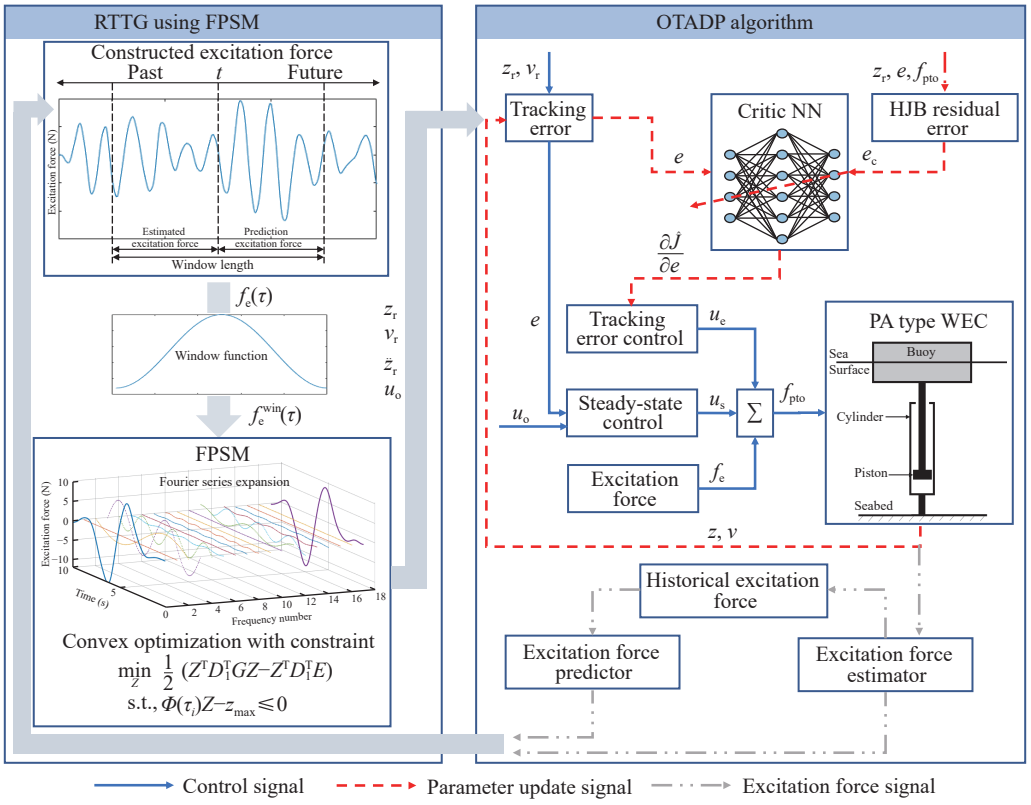

Figure 2 FPSM-OTADP framework.

A. RTTG Using FPSM

FPSM for WEC The optimization problem in Eq. (6) can be transformed into a convex one using the FPSM. The core idea of FPSM involves using the Fourier series to approximate each term in Eq. (5). Assuming that the perfect knowledge of excitation force f_e in $[0,T]$ is known and T is the period of f_e, the excitation force can be expanded in a Fourier series as

$$f_e(t) \approx a_{e,0} + \sum_{n=1}^{N-1}(a_{e,n}\cos\omega_n t + b_{e,n}\sin\omega_n t) \tag{7}$$

where $t \in [0,T]$, $\omega_n = n\omega_0$, $n \in [1, N-1]$, is the n-th angular frequency of harmonic sinusoid, $\omega_0 = 2\pi/T$ is the basic angular frequency, $a_{e,n}$ and $b_{e,n}$ are the coefficients of the harmonic sinusoids, and N is the dimension of the harmonic sinusoid.

The basic function vector is defined as

$$\Phi(t) := [1, \cos\omega_1 t, \cos\omega_2 t, \ldots, \cos\omega_{N-1} t, \sin\omega_1 t, \sin\omega_2 t, \ldots, \sin\omega_{N-1} t]^T \tag{8}$$

and the coefficient $E \in \mathbb{R}^{2N-1}$ is defined as

$$E := [a_{e,0}, a_{e,1}, a_{e,2}, \ldots, a_{e,N-1}, b_{e,1}, b_{e,2}, \ldots, b_{e,N-1}]^T \tag{9}$$

The excitation force can be represented as

$$f_e(t) = E^T \Phi(t) \tag{10}$$

Analogously, the displacement z and PTO force f_{pto} can also be approximated by basic function $\Phi(t)$

$$z = a_{z,0} + \sum_{n=1}^{N-1}(a_{z,n}\cos\omega_n t + b_{z,n}\sin\omega_n t) = Z^T \Phi(t) \tag{11}$$

$$f_{pto} = a_{u,0} + \sum_{n=1}^{N-1}(a_{u,n}\cos\omega_n t + b_{u,n}\sin\omega_n t) = U^T \Phi(t) \tag{12}$$

where $a_{z,n}$, $b_{z,n}$, $a_{u,n}$, and $b_{u,n}$ are the coefficients of the harmonic sinusoids, and Z and U are the Fourier series coefficients of displacement z and PTO force f_{pto}, respectively, which are denoted as

$$Z = [a_{z,0}, a_{z,1}, a_{z,2}, \ldots, a_{z,N-1}, b_{z,1}, b_{z,2}, \ldots, b_{z,N-1}]^T \tag{13}$$

and

$$U = [a_{u,0}, a_{u,1}, a_{u,2}, \ldots, a_{u,N-1}, b_{u,1}, b_{u,2}, \ldots, b_{u,N-1}]^{\mathrm{T}} \tag{14}$$

The buoy velocity v can be represented as

$$v = \dot{z} = \sum_{n=1}^{N-1} (b_{z,n}\omega_n \cos\omega_n t - a_{z,n}\omega_n \sin\omega_n t) = (D_1 Z)^{\mathrm{T}} \Phi(t) \tag{15}$$

where $D_1 = \begin{bmatrix} 0 & D_{11} \\ -D_{11}^{\mathrm{T}} & 0 \end{bmatrix}$, $D_{11}^{\mathrm{T}} = \begin{bmatrix} 0 & \omega_1 & 0 & \ldots & 0 \\ 0 & 0 & \omega_2 & \ldots & 0 \\ \vdots & \vdots & \vdots & \ddots & \vdots \\ 0 & 0 & 0 & \ldots & \omega_{N-1} \end{bmatrix}$.

Substituting Eqs. (11) and (12) into Eq. (6) and using the orthogonality of basic function, which is $\int_0^T \Phi(t)\Phi(t)^{\mathrm{T}} \mathrm{d}t/T = I/2$, where I is the identity matrix, the objective function in Eq. (6) can be simplified as

$$\min_{Z,U} \frac{1}{2} Z^{\mathrm{T}} D_1^{\mathrm{T}} U \tag{16}$$

Similarly, the buoy acceleration $\ddot{z}$ is

$$\ddot{z} = \sum_{n=1}^{N-1} (-a_{z,n}\omega_n^2 \cos\omega_n t - b_{z,n}\omega_n^2 \sin\omega_n t) = (D_2 Z)^{\mathrm{T}} \Phi(t) \tag{17}$$

where $D_2 = -\mathrm{diag}(0, \omega_1^2, \ldots, \omega_{N-1}^2, \omega_1^2, \ldots, \omega_{N-1}^2)$. Furthermore, inspired by Ref. [27], the convolutional term f_{r1} in Eq. (3) can also be approximated by the Fourier series

$$f_{r1} = (QZ)^{\mathrm{T}} \Phi(t) \tag{18}$$

where $Q = \begin{bmatrix} Q_1 & Q_2 \\ -Q_2^{\mathrm{T}} & Q_3 \end{bmatrix}$, and

$$Q_2^{\mathrm{T}} = \begin{bmatrix} 0 & 0 & \ldots & 0 \\ \omega_1 B(\omega_1) & 0 & \ldots & 0 \\ 0 & \omega_2 B(\omega_2) & \ldots & 0 \\ \vdots & \vdots & \ddots & \vdots \\ 0 & 0 & \ldots & \omega_{N-1} B(\omega_{N-1}) \end{bmatrix} \tag{19}$$

and $Q_1 = \mathrm{diag}(0, \mathcal{A}(\omega_1), \ldots, \mathcal{A}(\omega_{N-1}))$, $Q_3 = \mathrm{diag}(\mathcal{A}(\omega_1), \mathcal{A}(\omega_2), \ldots, \mathcal{A}(\omega_{N-1}))$, $\mathcal{A}(\omega_i) = -\omega_i^2 (A(\omega_i) - m_\infty)$, $i \in [1, N-1]$.

$A(\omega)$ and $B(\omega)$ are the frequency-domain representations of the added mass and radiation damping, respectively, and satisfy the Ogilvie relation [28]

$$A(\omega) = m_\infty - \frac{1}{\omega} \int_0^\infty k_r(t) \sin(\omega t) \mathrm{d}t \tag{20}$$

$$B(\omega) = \int_0^\infty k_r(t) \cos(\omega t) \mathrm{d}t \tag{21}$$

Hence, the coefficients of the Fourier series of PTO force f_{pto} can be further replaced by

$$U = m_t D_2 Z + k_{hs} Z + QZ - E \tag{22}$$

Then, substituting Eq. (22) into the objective function in Eq. (16), we find the objective function

$$\min_Z \frac{1}{2} (Z^{\mathrm{T}} D_1^{\mathrm{T}} G Z - Z^{\mathrm{T}} D_1^{\mathrm{T}} E) \tag{23}$$

where $G = m_t D_2 Z + Q + k_{hs} I$. Assuming that the sampling time is t_s and there are N_s sampling points in $[0, T]$, taking the limitation of displacement into account, we get

$$z_{\min} \leqslant Z^{\mathrm{T}} \Phi(n t_s) \leqslant z_{\max} \tag{24}$$

where $n = 0, 1, \ldots, N_s - 1$ and $t_s \in [0, T]$. Therefore, the optimization problem in Eq. (6) is

$$\min_Z \frac{1}{2} (Z^{\mathrm{T}} D_1^{\mathrm{T}} G Z - Z^{\mathrm{T}} D_1^{\mathrm{T}} E), \quad \text{s.t., Eq. (24)} \tag{25}$$

RH implementation of FPSM for RTTG When the reference trajectory is generated in an RH manner, the excitation force signal is non-periodic in each optimization. To eliminate the Gibbs phenomenon in trajectory generation, the window function is employed with the window interval $[t - (L/2)t_s, t + (L/2)t_s]$, where t is current time, L is the window length, and t_s is the sampling time, respectively.

The procedure of the RH implementation is shown in Algorithm 1.

Algorithm 1 Optimal trajectory online generation based on FPSM

Input: History excitation force $f_e(\tau_1), \tau_1 \in [t - (L/2)t_s, t]$, future excitation force $\hat{f}_e(\tau_2), \tau_2 \in [t + t_s, t + (L/2)t_s]$, and window function f_{win}.

Output: Present time reference trajectory z_r, v_r, $\ddot{z}_r$, and optimal control force u_o.

1: Construct the total excitation force $f_e(\tau) = f_e(\tau_1)$, $\tau = \tau_1$ and $f_e(\tau) = \hat{f}_e(\tau_2)$, $\tau = \tau_2$.

2: Apply window function to the excitation force signal $f_e^{win}(\tau) = f_{win}(\tau) \times f_e(\tau)$.

3: Convert the excitation force signal f_e^{win} to the Fourier series form to get the Fourier series coefficient E.

4: Optimize Eq. (25) and derive the $z_r^{win}(\tau)$, $v_r^{win}(\tau)$, $\ddot{z}_r^{win}(\tau)$, and $u_o^{win}(\tau)$.

5: Output the reference trajectory $z_r(t)$, $v_r(t)$, $\ddot{z}_r(t)$, and the optimal control force $u_o(t)$.

Remark 1 The RH implementation of FPSM is noncausal due to the requirement of future wave information. However, the short-term wave prediction techniques can address this issue [29, 30]. Here, we assume that the short-term future wave information is known.

B. OTADP Algorithm

Optimal control of WEC tracking problem Let the reference trajectories of displacement and velocity be z_r and v_r, respectively, and define the error vector as

$$e(t) = \begin{bmatrix} e_1 \\ e_2 \end{bmatrix} = \begin{bmatrix} z - z_r \\ v - v_r \end{bmatrix} \tag{26}$$

The goal of solving the WEC tracking problem is to find the optimal PTO force f_{pto}^* which can stabilize $e(t)$ to 0.

The PTO force f_{pto} can be divided into two parts: the steady-state control u_s and error-tracking control u_e, i.e.,

$$f_{pto} = u_s + u_e \tag{27}$$

The steady-state control is designed as

$$u_s = u_o - Ke(t) \tag{28}$$

where $K=[k_1,k_2]$, $k_1>0$ and $k_2>0$. The proportional term $Ke(t)$ is used to maintain the steady-state tracking performance. We denote that $f(z,v)=-k_{\mathrm{hs}}z-f_{\mathrm{r1}}$. Taking the derivative of Eq. (26), we get

$$\dot{e}(t)=\begin{bmatrix} e_2 \\ \frac{1}{m_{\mathrm{t}}}(f(z,v)+f_{\mathrm{e}}+u_{\mathrm{s}})-\ddot{z}_{\mathrm{r}} \end{bmatrix}+\begin{bmatrix} 0 \\ \frac{1}{m_{\mathrm{t}}} \end{bmatrix}u_{\mathrm{e}}= F(e)+B_{\mathrm{e}}u_{\mathrm{e}} \tag{29}$$

Hence, the tracking control for Eq. (1) is converted to a regulation control problem with regard to the error-tracking control, which serves to stabilize Eq. (29). It should be pointed out that $\ddot{z}_{\mathrm{r}}$ can also be derived by optimizing Eq. (25). Hence, we do not need the dynamics of the reference signals.

The performance function can be defined as

$$V(e)=\int_t^{\infty} e^{\mathrm{T}}Qe+ru_{\mathrm{e}}^2\mathrm{d}\tau \tag{30}$$

where Q is a positive definite matrix and r is a positive weight coefficient. Define the Hamiltonian function as

$$H\left(e,u_{\mathrm{e}},\frac{\partial V(e)}{\partial e}\right)=e^{\mathrm{T}}Qe+ru_{\mathrm{e}}^2+\left(\frac{\partial V(e)}{\partial e}\right)^{\mathrm{T}}\dot{e} \tag{31}$$

The optimal performance function $J(e)$ and optimal control policy u_{e}^* satisfy the Hamilton-Jacobi-Bellman (HJB) equation

$$H\left(e,u_{\mathrm{e}}^*,\frac{\partial J(e)}{\partial e}\right)=0 \tag{32}$$

Through the stationary condition [31]

$$\frac{\partial H(e,u_{\mathrm{e}}^*,\partial J(e)/\partial e)}{\partial u_{\mathrm{e}}^*}=0 \tag{33}$$

u_{e}^* is calculated by

$$u_{\mathrm{e}}^*(e)=-\frac{1}{2r}B_{\mathrm{e}}^{\mathrm{T}}\frac{\partial J(e)}{\partial e} \tag{34}$$

Substituting Eq. (34) into Eq. (32), we have

$$0=e^{\mathrm{T}}Qe+\left(\frac{\partial J(e)}{\partial e}\right)^{\mathrm{T}}F(e)-\frac{1}{4r}\left(\frac{\partial J(e)}{\partial e}\right)^{\mathrm{T}}B_{\mathrm{e}}B_{\mathrm{e}}^{\mathrm{T}}\frac{\partial J(e)}{\partial e} \tag{35}$$

It can be proven that the optimal value function is a Lyapunov function, which means that the optimal u_{e}^* can stabilize the error system in Eq. (29). Meanwhile, Eq. (35) is difficult to solve. An ADP approach is employed to solve Eq. (35).

OTADP algorithm design Based on the key idea of ADP, the optimal value function $J(e)$ is represented by a critic NN

$$J(e)=W^{*\mathrm{T}}\phi(e)+\xi(e) \tag{36}$$

where $W^*\in\mathbb{R}^{N_{\mathrm{c}}}$ is the unknown optimal constant weight, $\phi(e)\in\mathbb{R}^{N_{\mathrm{c}}}$ is the activation function vector with linear-independent elements, $\xi(e)$ is the reconstructed error, and N_{c} is the number of the critic NN's neurons, respectively. Based on the Weierstrass approximation theorem [32], as $N_{\mathrm{c}}\to\infty$, the reconstructed error $\xi(e)\to 0$. The common assumption about critic NN is given as follows:

Assumption 1 As mentioned in Ref. [33], the optimal weight W^*, activation function vector $\phi(e)$, reconstructed error $\xi(e)$, and their derivatives $\partial\phi(e)/\partial e$ and $\partial\xi(e)/\partial e$ are all bounded by $\|W^*\|\leqslant W_{\mathrm{c}}$, $\|\phi(e)\|\leqslant\phi_{\mathrm{c}}$, $\phi_{\mathrm{xcm}}\leqslant\|\partial\phi(e)/\partial e\|\leqslant\phi_{\mathrm{xcM}}$, and $\|\partial\xi(e)/\partial e\|\leqslant\xi_{\mathrm{xcM}}$, and the derivative of tracking error e is bounded by $\|\dot{e}\|\leqslant\chi_{\mathrm{M}}$, where W_{c} is the upper bound of the norm of the critic NN's optimal weights, ϕ_{c} is the upper bound of the norm of the critic NN's activation function vector, ϕ_{xcm} and ϕ_{xcM} are the lower bound and upper bound of the norm of the derivative of the critic NN's activation function vector respectively, ξ_{xcM} is the upper bound of the norm of the derivative of the critic NN's reconstructed error, and χ_{M} is the upper bound of the norm of the tracking error's derivative, and they are all positive numbers.

Based on Eq. (34), the optimal control policy becomes

$$u_{\mathrm{e}}^*(e)=-\frac{1}{2r}B_{\mathrm{e}}^{\mathrm{T}}\left(\frac{\partial\phi(e)}{\partial e}^{\mathrm{T}}W^*+\frac{\partial\xi(e)}{\partial e}\right) \tag{37}$$

However, the optimal weight W^* is unknown in practice. We can use the estimated version of W^*, noted as $\hat{W}$, to make $\hat{W}$ closer to W^*. Then the estimated value function will be

$$\hat{J}(e)=\hat{W}^{\mathrm{T}}\phi(e) \tag{38}$$

and the estimated control policy will be

$$\hat{u}_{\mathrm{e}}(e)=-\frac{1}{2r}B_{\mathrm{e}}^{\mathrm{T}}\frac{\partial\phi(e)}{\partial e}^{\mathrm{T}}\hat{W} \tag{39}$$

Denote $\nabla_e\phi=\partial\phi(e)/\partial e$ and $\nabla_e\xi=\partial\xi(e)/\partial e$. Equation (35) is restated as

$$0=e^{\mathrm{T}}Qe+W^{*\mathrm{T}}\nabla_e\phi F(e)-\frac{1}{4r}W^{*\mathrm{T}}\nabla_e\phi B_{\mathrm{e}}B_{\mathrm{e}}^{\mathrm{T}}\nabla_e\phi^{\mathrm{T}}W^*+\xi_{\mathrm{HJB}} \tag{40}$$

where $\xi_{\mathrm{HJB}}=\nabla_e^{\mathrm{T}}\xi F(e)-W^{*\mathrm{T}}\nabla_e\phi B_{\mathrm{e}}B_{\mathrm{e}}^{\mathrm{T}}\nabla_e\xi/(2r)-\nabla_e^{\mathrm{T}}\xi B_{\mathrm{e}}B_{\mathrm{e}}^{\mathrm{T}}\nabla_e\xi/(4r)$, which is related to the reconstructed error $\xi(e)$. Similarly, when the optimal value function is estimated by $\hat{J}(e)$, Eq. (40) becomes

$$e_{\mathrm{c}}=e^{\mathrm{T}}Qe+\hat{W}^{\mathrm{T}}\nabla_e\phi F(e)-\frac{1}{4r}\hat{W}^{\mathrm{T}}\nabla_e\phi B_{\mathrm{e}}B_{\mathrm{e}}^{\mathrm{T}}\nabla_e\phi^{\mathrm{T}}\hat{W} \tag{41}$$

where e_{c} is the residual error. Define the loss function as

$$E_{\mathrm{l}}=\frac{1}{2}e_{\mathrm{c}}^{\mathrm{T}}e_{\mathrm{c}} \tag{42}$$

Using the gradient descent method, the weight-tuning law is

$$\dot{\hat{W}}=-\alpha\frac{\sigma}{(1+\sigma^{\mathrm{T}}\sigma)^2}e_{\mathrm{c}} \tag{43}$$

where $\sigma=\nabla_e\phi(F(e)+B_{\mathrm{e}}\hat{u}_{\mathrm{e}})$, α is the learning rate, and $(1+\sigma^{\mathrm{T}}\sigma)^2$ is the normalization term, respectively [16]. Let the weight error be $\tilde{W}=W^*-\hat{W}$. Then the derivative of $\dot{\tilde{W}}$ is $-\dot{\hat{W}}$. From Eqs. (40) and (41), we get

$$-e_{\mathrm{c}}=\tilde{W}^{\mathrm{T}}\nabla_e\phi F(e)-\frac{1}{2r}W^{*\mathrm{T}}\nabla_e\phi B_{\mathrm{e}}B_{\mathrm{e}}^{\mathrm{T}}\nabla_e\phi^{\mathrm{T}}\tilde{W}+\frac{1}{4r}\tilde{W}^{\mathrm{T}}\nabla_e\phi B_{\mathrm{e}}B_{\mathrm{e}}^{\mathrm{T}}\nabla_e\phi^{\mathrm{T}}\tilde{W}+\xi_{\mathrm{HJB}} \tag{44}$$

To determine the dynamic of $\tilde{W}$, σ must be represented with respect to $\tilde{W}$

$$\sigma=\nabla_e\phi(F(e)+B_{\mathrm{e}}u_{\mathrm{e}}^*-B_{\mathrm{e}}(u_{\mathrm{e}}^*-\hat{u}_{\mathrm{e}}))=\nabla_e\phi\varpi+\frac{1}{2r}\nabla_e\phi B_{\mathrm{e}}B_{\mathrm{e}}^{\mathrm{T}}\nabla_e^{\mathrm{T}}\phi\tilde{W} \tag{45}$$

where $\varpi = F(e) + B_e u_e^* + B_e B_e^T \nabla_e \xi/(2r)$. Substituting Eqs. (43) and (45) into Eq. (44), the dynamic of $\tilde{W}$ is

$$\dot{\tilde{W}} = -\frac{\alpha}{(1+\sigma^T\sigma)^2}\left(\nabla_e\phi\varpi + \frac{1}{2r}\nabla_e\phi B_e B_e^T \nabla_e^T \phi \tilde{W}\right)\times \left(\tilde{W}^T\nabla_e\phi\varpi + \frac{1}{4r}\tilde{W}^T\nabla_e\phi B_e B_e^T \nabla_e \phi^T \tilde{W}\right) - \frac{\alpha}{(1+\sigma^T\sigma)^2}\left(\nabla_e\phi\varpi + \frac{1}{2r}\nabla_e\phi B_e B_e^T \nabla_e^T \phi \tilde{W}\right)\xi_{HJB} \quad (46)$$

The implementation of ADP tracking approach is shown in Algorithm 2.

Remark 2 As mentioned in Ref. [34], $\sigma/(1+\sigma^T\sigma)$ is required to satisfy the PE condition by adding the probing noise to the control policy. In this case, the excitation force acts on WEC, which satisfies the PE condition [18].

Algorithm 2 Implementation of FPSM-OTADP control

1: Set the start time $t = t_0$, control time as T, and sampling time as t_s. Determine the window function f_{win} and window length L. Choose the activation function $\phi(e)$ and the initial value of the estimated weight $\hat{W}$. Set control parameters as K and α.
2: **while** $t \leqslant T$ **do**
3: Measure the WEC displacement z and velocity v.
4: Compute the historical excitation force $f_e(\tau_1), \tau_1 \in [t-(L/2)t_s, t]$.
5: Predict the future excitation force $\hat{f}_e(\tau_2)$, $\tau_2 \in [t+t_s, t+(L/2)t_s]$.
6: Execute Algorithm 1 and get z_r, v_r, $\dot{z}_r$, and u_o.
7: Calculate the tracking error e, the residual error e_c using Eq. (41), and the normalized term $(1+\sigma^T\sigma)^2$.
8: Update the critic NN weight $\hat{W}$ using Eq. (43).
9: Update the error-tracking control $\hat{u}_e$ using Eq. (39).
10: Output the overall control force $f_{pto} = u_s + \hat{u}_e$.
11: Set $t = t + t_s$.
12: **end while**

C. Stability and Convergence Analysis

In this section, the stability of the error system in Eq. (29) and the convergence of $\tilde{W}$ will be discussed.

Theorem 1 Considering the error system in Eq. (29) and the dynamics of the estimation error of weights in Eq. (46) with PE condition satisfied, if Assumption 1 holds, the weight-tuning law is expressed as (43) and the estimated control policy is expressed as (39). Then, the tracking error e and the estimation error of weight $\tilde{W}$ are uniformly ultimately bounded (UUB). Moreover, the estimated control policy $\hat{u}_e$ will converge to the neighborhood of the optimal control policy u_e^* uniformly.

The proof of Theorem 1 is presented in Appendix.

IV. Simulation Experiment

In this section, a 1:50 cylindrical heaving buoy model in Ref. [35] is adopted to validate the proposed FPSM-based OTADP algorithm. The parameters of WEC model are summarized in Table 1.

The state-space descriptions of the radiation impulse function in Eq. (4) are

$$A_r = \begin{bmatrix} -3.1848 & -4.3372 & -3.1009 \\ 4.3372 & -0.0875 & -0.3882 \\ 3.1009 & -0.3882 & -2.8499 \end{bmatrix},$$

$$B_r = \begin{bmatrix} -40.6964 \\ 5.9737 \\ 16.2722 \end{bmatrix},$$

$$C_r = \begin{bmatrix} -0.4070 & -0.0597 & -0.1627 \end{bmatrix}.$$

Based on Eq. (20), $A(\omega)$ and $B(\omega)$ are approximated as follows

$$A(\omega) = 87.010\exp\left[-\left(\frac{\omega+40.280^2}{26.730}\right)\right] + 4.716\exp\left[-\left(\frac{\omega-12.910^2}{7.092}\right)\right],$$

$$B(\omega) = 4.594\exp\left[-\left(\frac{\omega-4.225}{2.816}\right)^2\right].$$

Table 1 WEC parameter.

Parameter	Symbol	Value
Density of water	ρ	1000 kg/m^3
Gravitational acceleration	g	9.81 m/s^2
Radius of the buoy	r_b	0.15 m
Draught of the buoy	d	0.28 m
Water plane area of the buoy	S	0.0707 m^2
Buoy mass	m	19.79 kg
Added mass at infinite frequency	m_∞	6.58 kg
Upper bound of displacement	z_{max}	0.28 m
Lower bound of displacement	z_{min}	−0.28 m

To show the capability of FPSM-OTADP in an irregular wave environment, we choose two irregular wave signals. Case 1 is the JONSWAP wave spectrum with significant wave height $H_s = 0.1$ m, peak period $T_p = 1.2$ s, and spectrum peak factor $\Gamma = 3.3$, respectively [36]. Case 2 is the real wave data. The wave profiles of two cases are shown in Fig. 3. The simulation time T is 300.0 s. The sampling time is set to $t_s = 0.1$ s. All simulations are conducted in MATLAB 2020b.

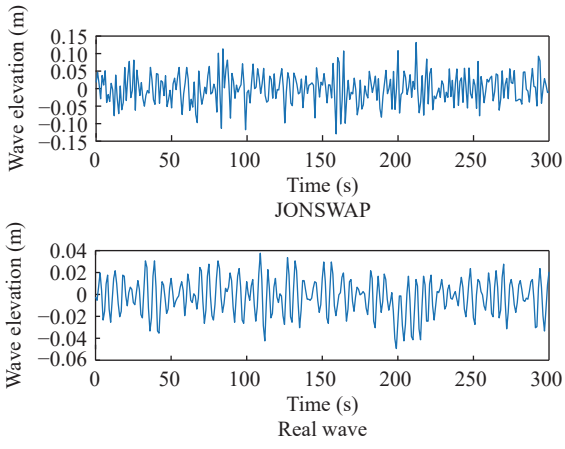

Figure 3 Wave profile of two cases.

A. Window Function and Window Length Determination of FPSM

For $t_s = 0.1$ s, the window length is set to $L = 100, 100 + \Delta L, \ldots, 500$, $\Delta L = 20$. The window functions are chosen from the rectangular window, the Tukey window with $r = 0.25$, 0.50, 0.75, 1.00, and the Hamming window. The mean square errors (MSEs) $\sum_{i=1}^{n} (\hat{x}_i - x_i^*)/n$ of the average power, displacement, and velocity $\hat{x}_i$ with respect to their optimal values x_i^* are shown in Figs. 4 and 5, respectively.

For case 1, when $L \leqslant 240$, the MSE values decrease to zero with some fluctuations. When $L > 240$, the MSE values have divergence tendencies. Hence, the window length of 240 is chosen. Similarly, the window length of case 2 is 200. Among these window functions, it can be observed that the Hamming window yields a balanced performance in measuring MSEs of the average power, displacement, and velocity in both case 1 and case 2. Thus, the Hamming window function is selected for both cases in the following simulation.

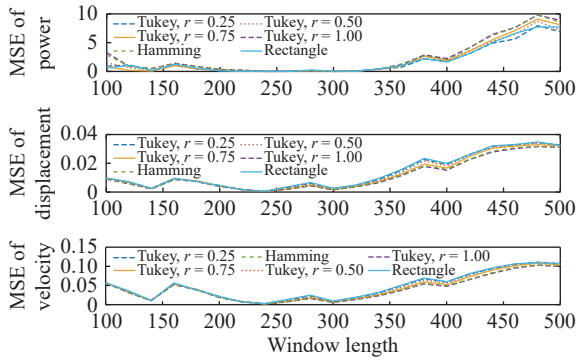

Figure 4 MSE between optimal values and RH implemented values for case 1 with $t_s = 0.1$ s.

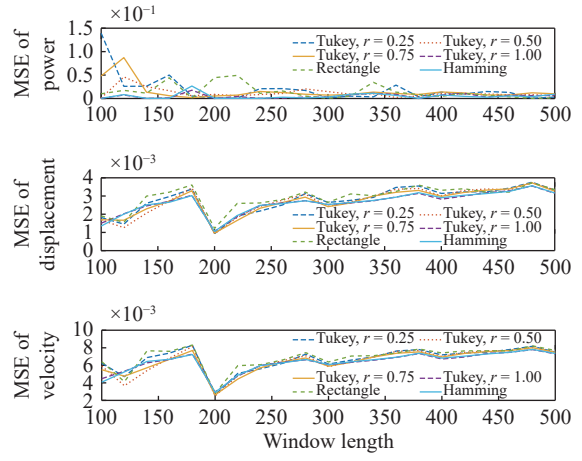

Figure 5 MSE between optimal values and RH implemented values for case 2 with $t_s = 0.1$ s.

B. FPSM-OTADP Simulation Result

To compare the trajectory tracking and energy absorption performances, the optimal trajectory and extracted energy are calculated offline. The dimension N of the Fourier series is set to 150.

Case 1 The activation function of critic NN is set to $\phi(e) = \left[e_1^2; e_1 e_2; e_2^2\right]$ with all initial weights being zero. Q and r in cost function are $Q = \text{diag}(10, 10)$ and $r = 0.005$, respectively. The controller parameters are set to $\alpha = 30$ and $K = 26.37$. The approximate dimension N in RH implementation is set to 10. The tracking performances and extracted energy of an offline computed optimal trajectory are shown in Fig. 6. The tracking error is close to zero in 5 s and the extracted energy of WEC approaches to the optimal energy, which validates the proposed algorithm for energy maximization condition.

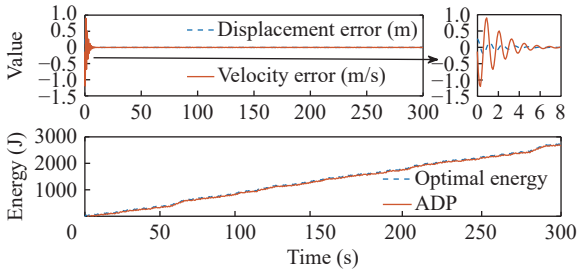

Figure 6 Tracking error and extracted energy under the optimal trajectory of case 1.

The results of RH implementation of FPSM are shown in Fig. 7. The tuning of critic NN weights (W_1, W_2, and W_3) is demonstrated in Fig. 8, in which the upper part presents the optimal trajectory and the lower part presents the RH implementation of FPSM, respectively. The converged weights are [0.4264; −4.2750; 0.1081]. Due to the conflict between online computation and approximation accuracy requirement, even though Fig. 4 illustrates that the chosen window function and window length have the lowest MSE of power and trajectory, the computed wave excitation force differs from the real wave excitation force. Hence, a sudden change occurs in the generated trajectory. The greatest sudden change can be observed in Fig. 7 at 176 s. Under OTADP, the tracking errors reach zero at 182 s. The critic NN weights in Fig. 8 converge to the optimal values, which shows the robustness of the FPSM-OTADP algorithm.

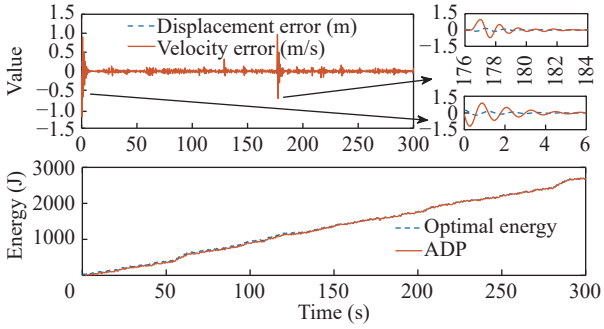

Figure 7 Tracking error and extracted energy under RH implementation of FPSM for case 1.

To demonstrate the effectiveness of tracking ability of FPSM-OTADP, we compare FPSM-OTADP with sliding mode control (SMC) and backstepping (BS) control [22], which are commonly used in WEC real-time control. The

tracking performances of these three methods are shown in Fig. 9. The parameters of SMC and BS methods are adjusted to make WEC track the optimal trajectory accurately and to obtain the maximum energy using the optimal trajectory. As shown in Fig. 9, both SMC and BS have poorer tracking performances compared with the proposed OTADP method. Displacement errors indicate that under the control of SMC and BS, WEC often jumps out of the water or becomes fully submerged, which increases the risk of damage to the WEC device. The performance indices are the sum of absolute errors (SAEs), where $\mathrm{SAE}(x, x_\mathrm{r}) = \sum_{i=0}^{n-1} |x_i - x_{\mathrm{r},i}|$, x_r represents the vector of the reference values of the displacement, velocity, and PTO force, x represents the vector of their real values, and subscript i means the i-th element of the vector. The indices are summarized in Table 2.

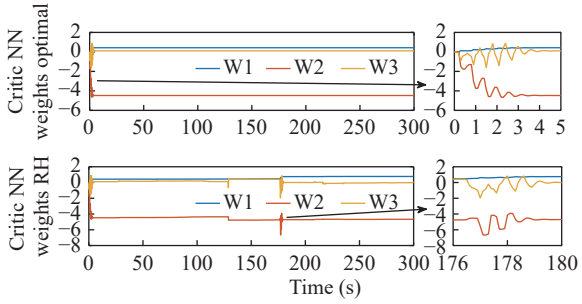

Figure 8 Critic NN weights of case 1.

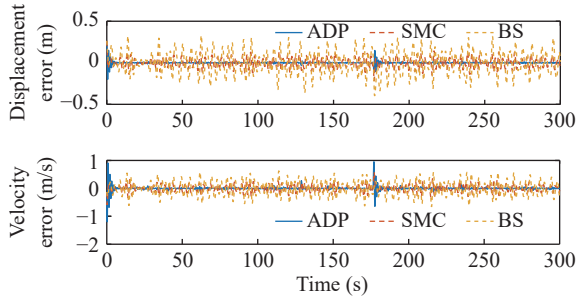

Figure 9 Tracking performance comparison for case 1.

Table 2 Tracking control performance of case 1.

Method	SAE(z, z_r) (m)	SAE(v, v_r) (m/s)	SAE(u, u_o) (N)
ADP	44.14	130.19	1.94×10^4
SMC	148.22	326.16	8.28×10^4
BS	335.31	618.36	2.03×10^5

Case 2 Similar to case 1, the activation function of critic NN is set to $\phi(e) = \left[e_1^2; e_1e_2; e_2^2\right]$ and the initial weights of critic NN are all zero. Q and r in cost function are $Q = \mathrm{diag}(10, 10)$ and $r = 0.010$, respectively. The controller parameters are set to $\alpha = 50$ and $K = 26.37$. The approximate dimension N in RH implementation is set to 12, and window function is set as Hamming window with a length of 200. The initial states of WEC are all zero. Under the optimal reference trajectory, the tracking performances and extracted energy results are shown in Fig. 10. The results also show that the proposed algorithm can cause WEC to track the optimal trajectory and obtain the maximum energy in ideal conditions.

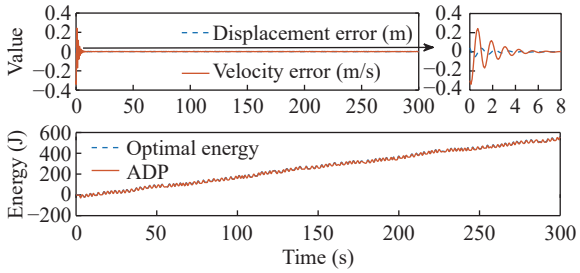

Figure 10 Tracking error and extracted energy under the optimal trajectory of case 2.

The tracking error and the extracted energy under RH implementation of FPSM are depicted in Fig. 11. The comparison of the three methods is shown in Fig. 12.

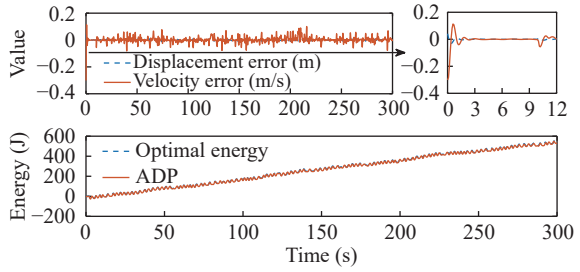

Figure 11 Tracking error and extracted energy under RH implementation of FPSM for case 2.

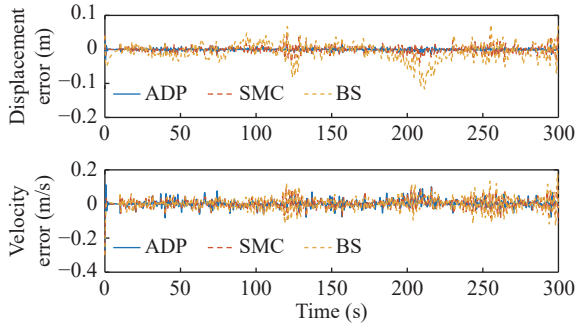

Figure 12 Tracking performance comparison for case 2.

The tracking performance indices are listed in Table 3. In this case, the FPSM-OTADP algorithm has the displacement tracking performance that can satisfy the displacement constraints, while the velocity tracking errors have many fluctuations due to the sudden change in the generated trajectory.

Table 3 Tracking control performance of case 2.

Method	SAE(z, z_r) (m)	SAE(v, v_r) (m/s)	SAE(u, u_o) (N)
ADP	61.07	199.91	4.41×10^5
SMC	67.38	144.12	4.93×10^5
BS	82.08	95.63	4.71×10^5

Under the optimal trajectory, the critic NN weights converge to [0.0747; −0.4663; 0.6617], as shown in the upper part of Fig. 13. For RH implementation of FPSM, the critic NN weights can still converge under the sudden change of the generated trajectory.

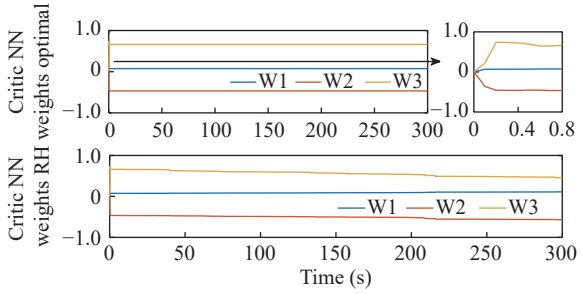

Figure 13 Critic NN weights of case 2.

The tracking performance shows that FPSM-OTADP can track the desired trajectory while ensuring WEC to satisfy displacement constraints. To further show the ability of absorbing energy of FPSM-OTADP, two noncausal WEC absorbing energy control methods are compared with the proposed approach. One is the linear noncausal optimal control (LNOC) [13], and the other is the improved model predictive control (IMPC) [10]. The results are shown in Fig. 14 and summarized in Table 4. In case 1, the extracted energy ratio of FPSM-OTADP is larger than that of LNOC by 5% and larger than that of IMPC by 26%. In case 2, due to the small wave profile, the extracted energy difference is small. However, in both cases, LNOC and IMPC extract lower energy compared with FPSM-OTADP. The results in both cases show the tracking ability of FPSM-OTADP algorithm and the safety assurance it provided for WEC, by accommodating the maximal absorption of WEC and ensuring long-term operation.

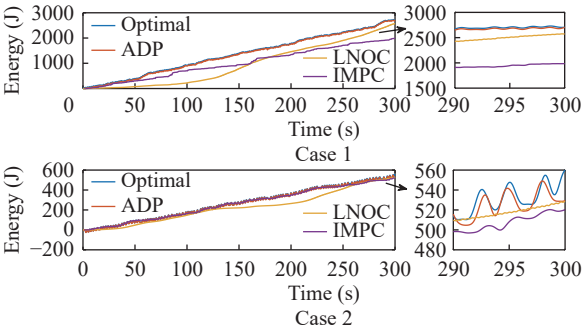

Figure 14 Extracted energy of cases 1 and 2.

Table 4 Extracted energy of cases 1 and 2.

Approach	Extracted energy (J)		Extracted energy ratio (%)	
	Case 1	Case 2	Case 1	Case 2
ADP	2702.7	529.5	99	94
LNOC	2574.8	528.7	94	94
IMPC	1984.6	520.9	73	92

The simulations are conducted on a computer with an Intel (R) Core (TM) i7-6700K, 4.00 GHz CPU, with a 16 GB memory. At each sampling time, RH implementation of FPSM using the fmincon function in MATLAB with sequence quadratic program (SQP) method takes 0.019 s to calculate the error-tracking control force u_e by solving the ode4 function, and the ADP-tracking algorithm takes 0.020 s. The total computing time is lower than the sampling time. Therefore, FPSM-OTADP can be used in the real-time control of WEC to enhance its energy absorption capacity.

V. Conclusion

This paper proposes a two-level control structure incorporating FPSM and OTADP algorithms to realize maximized energy absorption for WEC. The constrained optimal problem of WEC is converted into an optimal reference trajectory tracking problem by FPSM. The optimal reference trajectory is generated online by handling the constraints explicitly and utilizing the wave-prediction technique. To solve the trajectory tracking problem, the HJB equation is solved online using the OTADP algorithm, where a single critic NN is used to approximate the optimal value function and calculate the error-tracking control. We prove the convergence of the critic NN weights and the stability of the error-tracking system theoretically. Simulation results demonstrate the efficacy of the proposed FPSM-OTADP algorithm in terms of energy absorption and constraint avoidance based on realistic sea conditions. Additionally, the efficient computational time of FPSM-OTADP makes this approach feasible in practical implementation of WEC control.

Appendix
Proof of Theorem 1

Proof For convenience, let $\kappa = 1 + \sigma^{\mathrm{T}}\sigma$ and $\beta = \nabla_e \phi B_e B_e^{\mathrm{T}} \nabla_e \phi^{\mathrm{T}}$. Choose the candidate Lyapunov function as

$$J = J_1 + J_2 = \frac{1}{2}\alpha^{-1}\tilde{W}^{\mathrm{T}}\tilde{W} + \frac{1}{2}\gamma e^{\mathrm{T}} e + \varsigma J(e) \tag{A1}$$

where γ and ς are both positive weight coefficients. The derivative of J_1 is

$$\begin{aligned}\dot{J}_1 = {} & \alpha^{-1}\tilde{W}^{\mathrm{T}}\dot{\tilde{W}} = \\ & -\frac{1}{k^2}(\tilde{W}^{\mathrm{T}}\nabla_e \phi \varpi)^2 - \frac{3}{4r\kappa^2}\tilde{W}^{\mathrm{T}}\nabla_e \phi \varpi \tilde{W}^{\mathrm{T}}\beta\tilde{W} - \\ & \frac{1}{8r^2\kappa^2}(\tilde{W}^{\mathrm{T}}\beta\tilde{W})^2 - \frac{1}{\kappa^2}\tilde{W}^{\mathrm{T}}\nabla_e \phi \varpi \xi_{\mathrm{HJB}} - \\ & \frac{1}{2r\kappa^2}\tilde{W}^{\mathrm{T}}\beta\tilde{W}\xi_{\mathrm{HJB}}\end{aligned} \tag{A2}$$

Using the method of completing square and zooming, we get

$$\begin{aligned}\dot{J}_1 \leqslant {} & -\frac{1}{32\kappa^2}\|\tilde{W}\|^4 \phi_{\mathrm{xcm}}^4 B_c^2 + \Theta_1 + (\Theta_2 + \xi_{\mathrm{xcM}}^2)\|u_e^*\|^2 + \\ & \Theta_3 + \frac{1156r^2}{B_c^4\kappa^2}\|u_e^*\|^4\end{aligned} \tag{A3}$$

where

$$\Theta_1 = \frac{1156r^2}{B_c^4\kappa^2}\left(\eta + \frac{1}{2r}B_c^2\xi_{\mathrm{xcM}}\right)^4 \tag{A4}$$

$$\Theta_2 = \frac{2312r^2}{B_c^4\kappa^2}(\eta + \frac{1}{2r}B_c^2\xi_{xcM})^2 \tag{A5}$$

$$\Theta_3 = \frac{3}{2\kappa^2}(\xi_{xcM}\eta + \frac{1}{4}B_c^2\xi_{xcM}^2)^2 \tag{A6}$$

B_c is the norm of B and η is the bound of $F(e)$.

The derivative of J_2 is

$$\begin{aligned}\dot{J}_2 &= \gamma e^T\dot{e} + \varsigma\dot{J}(e) \leqslant \\ &\left(\frac{\gamma+2r\gamma}{2r} - \varsigma\lambda_{\min}(Q)\right)\|e\|^2 + \frac{\gamma}{4r}\|\tilde{W}\|^2\phi_{xcM}^2B_c^4 + \\ &\frac{\gamma}{4r}\xi_{xcM}^2B_c^4 + \left(\frac{\gamma}{2} - \varsigma r\right)\|u_e^*\|^2 + \frac{\gamma}{2}\eta^2\end{aligned} \tag{A7}$$

where $\lambda_{\min}$ is the minimum eigenvalue of Q. Substituting Eqs. (A3)–(A7) into Eq. (A1), we get

$$\begin{aligned}\dot{J} &\leqslant \dot{J}_1 + \dot{J}_2 \leqslant \\ &-\frac{1}{32\kappa^2}\|\tilde{W}\|^4\phi_{xcm}^4B_c^2 + \Theta_1 + \Theta_3 + \frac{1156r^2}{B_c^4\kappa^2}\|u_e^*\|^4 + \\ &\left(\frac{\gamma+2r\gamma}{2r} - \varsigma\lambda_{\min}(Q)\right)\|e\|^2 + \frac{\gamma}{4r}\|\tilde{W}\|^2\phi_{xcM}^2B_c^4 + \\ &\frac{\gamma}{4r}\xi_{xcM}^2B_c^4 + \left(\frac{\gamma}{2} - \varsigma r + \Theta_2 + \xi_{xcM}^2\right)\|u_e^*\|^2 + \frac{\gamma}{2}\eta^2\end{aligned} \tag{A8}$$

Define $\alpha_1 = \phi_{xcm}^2B_c/8$ and $\alpha_2 = \gamma\phi_{xcM}^2B_c^4/4r$. Then, we have

$$\begin{aligned}&-\frac{1}{32\kappa^2}\|\tilde{W}\|^4\phi_{xcm}^4B_c^2 + \frac{\gamma}{4r}\|\tilde{W}\|^2\phi_{xcM}^2B_c^4 = \\ &-\alpha_1^2\|\tilde{W}\|^4 - \left(\alpha_1\|\tilde{W}\|^2 - \frac{\alpha_2}{\alpha_1}\right)^2 + \left(\frac{\alpha_2}{\alpha_1}\right)^2\end{aligned} \tag{A9}$$

From Eq. (37), $\|u_e^*\|$ satisfies

$$\|u_e^*\| \leqslant \frac{1}{2r}B_c(\phi_{xcM}\|W^*\| + \xi_{xcM}) = \Gamma_3 \tag{A10}$$

Then, Eq. (A8) is written as

$$\dot{J} \leqslant -\alpha_1^2\|\tilde{W}\|^4 + \alpha_3\|e\|^2 + \Theta_1 + \Theta_3 + \Theta_4 \tag{A11}$$

where $\alpha_3 = (\gamma + 2r\gamma)/2r - \varsigma\lambda_{\min}(Q)$ and

$$\begin{aligned}\Theta_4 &= \frac{1156r^2}{B_c^4\kappa^2}\Gamma_3^4 + \frac{\gamma}{4r}\xi_{xcM}^2B_c^4 + \\ &\left(\frac{\gamma}{2} - \varsigma r + \Theta_2 + \xi_{xcM}^2\right)\Gamma_3^2 + \frac{\gamma}{2}\eta^2 + \left(\frac{\alpha_2}{\alpha_1}\right)^2\end{aligned} \tag{A12}$$

To promise the stability of Eqs. (29) and (46), α_3 should be negative and $\gamma/2 - \varsigma r + \Theta_2 + \xi_{xcM}^2$ should be positive. Hence, the parameters satisfy the following conditions

$$\varsigma \in \left(\frac{1+2r}{2r\lambda_{\min}(Q)}\gamma, \frac{\gamma + 2\Theta_2 + 2\xi_{xcM}^2}{2r}\right) \tag{A13}$$

$$r \leqslant \frac{\lambda_{\min}(Q) - 1}{2} \tag{A14}$$

$$\lambda_{\min}(Q) > 1 \tag{A15}$$

Since $\Theta_1 + \Theta_3 + \Theta_4 > 0$ and $\alpha_3 < 0$, for any

$$\|\tilde{W}\| > \sqrt[4]{\frac{\Theta_1 + \Theta_3 + \Theta_4}{\alpha_1^2}} \tag{A16}$$

$$\|e\| > \sqrt{\frac{\Theta_1 + \Theta_3 + \Theta_4}{-\alpha_3}} \tag{A17}$$

it can be proved that Eq. (A8) is negative. From the Lyapunov theorem, we can conclude that both the tracking error e and the critic NN weights error $\tilde{W}$ are uniformly ultimately bounded.

Moreover, the error between the estimated control $\hat{u}_e$ and optimal control u_e^* is

$$u_e^* - \hat{u}_e = -\frac{1}{2r}B_e^T\nabla_e\phi^T\tilde{W} - \frac{1}{2r}B_e^T\nabla_e\xi \tag{A18}$$

The norm of Eq. (A18) is

$$\|u_e^* - \hat{u}_e\| \leqslant \frac{1}{2r}B_c\phi_{xcM}\|\tilde{W}\| + \frac{1}{2r}B_c\xi_{xcM} \tag{A19}$$

When $\tilde{W}$ converges to the neighborhood of zero, it is apparently that $\|u_e^* - \hat{u}_e\|$ will reach the neighborhood of zero. The proof is completed. ■

ACKNOWLEDGMENT

This work was supported by the Key R&D Program of Shandong Province, China (No. 2021ZLGX04) and the Taishan Industrial Experts Programme (No. tsls20231203).

REFERENCES

[1] B. Guo and J. V. Ringwood, A review of wave energy technology from a research and commercial perspective, *IET Renew. Power Gen.*, 2021, 15(14), 3065–3090.

[2] B. G. Reguero, I. J. Losada, and F. J. Mendez, A global wave power resource and its seasonal, interannual and long-term variability, *Appl. Energy*, 2015, 148, 366–380.

[3] D. Gallutia, M. T. Fard, M. G. Soto, and J. He, Recent advances in wave energy conversion systems: From wave theory to devices and control strategies, *Ocean Eng.*, 2022, 252, 111105.

[4] A. Babarit and A. H. Clément, Optimal latching control of a wave energy device in regular and irregular waves, *Appl. Ocean Res.*, 2006, 28(2), 77–91.

[5] A. Babarit, M. Guglielmi, and A. H. Clément, Declutching control of a wave energy converter, *Ocean Eng.*, 2009, 36(12–13), 1015–1024.

[6] J. V. Ringwood, Wave energy control: Status and perspectives 2020, *IFAC-PapersOnLine*, 2020, 53(2), 12271–12282.

[7] J. Hals, J. Falnes, and T. Moan, Constrained optimal control of a heaving buoy wave-energy converter, *J. Offshore Mech. Arct. Eng.*, 2011, 133(1), 011401.

[8] G. Li and M. R. Belmont, Model predictive control of sea wave energy converters—Part I: A convex approach for the case of a single device, *Renew. Energy*, 2014, 69, 453–463.

[9] M. Richter, M. E. Magaña, O. Sawodny, and T. K. A. Brekken, Power optimisation of a point absorber wave energy converter by means of linear model predictive control, *IET Renew. Power Gen.*, 2014, 8(2), 203–215.

[10] Z. Wang, F. Luan, and N. Wang, An improved model predictive control method for wave energy converter with sliding mode control, *Ocean Eng.*, 2021, 240, 109881.

[11] G. Li, G. Weiss, M. Mueller, S. Townley, and M. R. Belmont, Wave energy converter control by wave prediction and dynamic programming, *Renew. Energy*, 2012, 48, 392–403.

[12] S. R. K. Nielsen, Q. Zhou, M. M. Kramer, B. Basu, and Z. Zhang, Optimal control of nonlinear wave energy point converters, *Ocean Eng.*, 2013, 72, 176–187.

[13] S. Zhan and G. Li, Linear optimal noncausal control of wave energy converters, *IEEE Trans. Control Syst. Technol.*, 2018, 27(4), 1526–1536.

[14] Y. Jia, K. Meng, L. Dong, T. Liu, C. Sun, and Z. Y. Dong, Economic model predictive control of a point absorber wave energy converter, *IEEE Trans. Sustain. Energy*, 2021, 12(1), 578–586.

[15] A. Al-Tamimi, F. L. Lewis, and M. Abu-Khalaf, Discrete-time nonlinear HJB solution using approximate dynamic programming: Convergence proof, *IEEE Trans. Syst. Man Cybern. Part B Cybern.*, 2008, 38(4), 943–949.

[16] H. Modares and F. L. Lewis, Optimal tracking control of nonlinear partially-unknown constrained-input systems using integral reinforcement learning, *Automatica*, 2014, 50(7), 1780–1792.

[17] C. Li, J. Ding, F. L. Lewis, and T. Chai, A novel adaptive dynamic programming based on tracking error for nonlinear discrete-time systems, *Automatica*, 2021, 129, 109687.

[18] J. Na, G. Li, B. Wang, G. Herrmann, and S. Zhan, Robust optimal control of wave energy converters based on adaptive dynamic programming, *IEEE Trans. Sustain. Energy*, 2019, 10(2), 961–970.

[19] J. Na, B. Wang, G. Li, S. Zhan, and W. He, Nonlinear constrained optimal control of wave energy converters with adaptive dynamic programming, *IEEE Trans. Ind. Electron.*, 2019, 66(10), 7904–7915.

[20] S. Zhan, J. Na, and G. Li, Nonlinear noncausal optimal control of wave energy converters via approximate dynamic programming, *IEEE Trans. Ind. Inf.*, 2019, 15(11), 6070–6079.

[21] G. Bacelli and J. V. Ringwood, Nonlinear optimal wave energy converter control with application to a flap-type device, *IFAC Proc. Vol.*, 2014, 47(3), 7696–7701.

[22] R. Genest and J. V. Ringwood, Receding horizon pseudospectral control for energy maximization with application to wave energy devices, *IEEE Trans. Control Syst. Technol.*, 2017, 25(1), 29–38.

[23] N. Faedo, G. Scarciotti, A. Astolfi, and J. V. Ringwood, Nonlinear energy-maximizing optimal control of wave energy systems: A moment-based approach, *IEEE Trans. Control Syst. Technol.*, 2021, 29(6), 2533–2547.

[24] C. Auger, A. Mérigaud, and J. V. Ringwood, Receding-horizon pseudo-spectral control of wave energy converters using periodic basis functions, *IEEE Trans. Sustain. Energy*, 2019, 10(4), 1644–1652.

[25] W. E. Cummins, The impulse response function and ship motions, *Schiffstechnik*, 1962, 9, 101–109

[26] A. Babarit and G. Delhommeau, Theoretical and numerical aspects of the open source BEM solver NEMOH, in *Proc. 11th European Wave and Tidal Energy Conference*, Nantes, France, 2015.

[27] A. Mérigaud and J. V. Ringwood, Optimal trajectories, nonlinear models and constraints in wave energy device control, *IFAC-PapersOnLine*, 2017, 50(1), 15645–15650.

[28] T. F. Ogilvie, Recent progress toward the understanding and prediction of ship motions, in *Proc. 5th Symposium on Naval Hydrodynamics*, Bergen, Norway, 1964, 3–79.

[29] Y. Pena-Sanchez, A. Merigaud, and J. V. Ringwood, Short-term forecasting of sea surface elevation for wave energy applications: The autoregressive model revisited, *IEEE J. Oceanic Eng.*, 2020, 45(2), 462–471.

[30] A. F. Davis and B. C. Fabien, Wave excitation force prediction of a heaving wave energy converter, *IEEE J. Oceanic Eng.*, 2021, 46(2), 564–572.

[31] F. L. Lewis and D. Liu, *Reinforcement Learning and Approximate Dynamic Programming for Feedback Control*. Hoboken, NJ, USA: John Wiley & Sons, 2013.

[32] M. H. Stone, The generalized weierstrass approximation theorem, *Math. Mag.*, 1948, 21(5), 237–254.

[33] J. Lu, Q. Wei, and F.-Y. Wang, Parallel control for optimal tracking via adaptive dynamic programming, *IEEE/CAA J. Autom. Sin.*, 2020, 7(6), 1662–1674.

[34] K. G. Vamvoudakis and F. L. Lewis, Online actor-critic algorithm to solve the continuous-time infinite horizon optimal control problem, *Automatica*, 2010, 46(5), 878–888.

[35] B. Guo, R. Patton, S. Jin, J. Gilbert, and D. Parsons, Nonlinear modeling and verification of a heaving point absorber for wave energy conversion, *IEEE Trans. Sustain. Energy*, 2018, 9(1), 453–461.

[36] K. Hasselmann, T. P. Barnett, E. Bouws, H. Carlson, D. E. Cartwright, K. Enke, J. A. Ewing, H. Gienapp, D. E. Hasselmann, P. Kruseman et al., Measurements of wind-wave growth and swell decay during the joint north sea wave project (JONSWAP), *Ergaenzungsheft Zur Deutschen Hydrographischen Zeitschrift, Reihe A*, 1973.

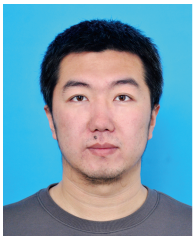

Xinyu Bao received the BS and MS degrees from Ocean University of China, Qingdao, China, in 2016 and 2023, respectively. He is currently a teaching assistant at Department of Railway, Hohhot Vocational College, Hohhot, China. His research interests include adaptive learning control and high-speed train control and scheduling.

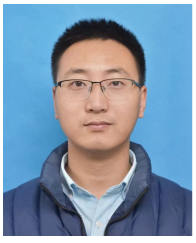

Zhen Chen received the BS and MS degrees from Ocean University of China, Qingdao, China, in 2012 and 2015, respectively. He is currently an engineer at Automation and Measurement Department, Ocean University of China, Qingdao, China. His research interests include intelligent control, ocean measurement, and control technology.

Ming Li received the BS and PhD degrees in control theory and control engineering from Northeastern University, Shenyang, China, in 1997 and 2003, respectively. From 2003 to 2006, he was a postdoctoral fellow at Electric Automation Institute, Northeastern University, China. In 2006, he joined College of Engineering, Ocean University of China, Qingdao, China. Since 2013, he is a full professor at Automation and Measurement Department, Ocean University of China, Qingdao, China. He is the author of 3 books, more than 70 articles, and more than 10 inventions. His research interests include intelligent signal processing and control and ocean energy power system modeling and control.